Analytical and Bioanalytical Chemistry (2022) 414:6149–6156
https://doi.org/10.1007/s00216-022-04180-7

RESEARCH PAPER

Telomere G-triplex lights up Thioflavin T for RNA detection: new wine in an old bottle

Shanshan Qin[1,2] · Xuliang Chen[3] · Zhichen Xu[1,2] · Tao Li[1,2] · Shuhong Zhao[2,4] · Rui Hu[1,2] · Jiang Zhu[1,2] · Ying Li[1,2] · Yunhuang Yang[1,2] · Maili Liu[1,2]

Received: 19 May 2022 / Revised: 6 June 2022 / Accepted: 13 June 2022 / Published online: 21 June 2022

Abstract

Few reports are found working on the features and functions of the human telomere G-triplex (ht-G3) though the telomere G-quadruplex has been intensely studied and widely implemented to develop various biosensors. We herein report that ht-G3 lights up Thioflavin T (ThT) and establish a sensitive biosensing platform for RNA detection by introducing a target recycling strategy. An optimal condition was selected out for ht-G3 to promote ThT to generate a strong fluorescence. Accordingly, an ht-G3-based molecular beacon was successfully designed against the corresponding RNA sequence of the SARS-CoV-2 N-gene. The sensitivity for the non-amplified RNA target achieves 0.01 nM, improved 100 times over the conventional ThT–based method. We believe this ht-G3/ThT–based label-free strategy could be widely applied for RNA detection.

Keywords G-triplex · Thioflavin T · RNA detection · Label-free detection · Biosensor · Target recycling

Introduction

Guanine-rich oligonucleotide sequences can fold into four-stranded DNA structures termed G-quadruplex (G4) through Hoogsteen hydrogen bonds [1–3]. G4s widely present in human genome and play important roles in gene transcription, replication, translation regulation, maintaining genome stability [4, 5], and others [6–8]. In addition to the physiological functions, G4s also possess unique biochemical properties such as binding with Thioflavin T (ThT) or hemin [9], which have been widely employed to develop a label-free fluorescent light-on or peroxidase-like enzyme probe, named molecular beacon (MB). For example, Guan et al. reported a strategy to use a ThT derivative to visualize DNA and RNA G4 structures with promising affinity and selectivity [10].

As an important element of the biosensing platform, G4 commonly functions as the signal transducer due to its sensitivity to environmental stimuli and its stability in metal ion solutions (e.g., Na^+, K^+). However, the too-stable G4 structures could bring some problems in cases requiring the rearrangement of the high-order structure during target DNA or RNA binding [11–13]. Therefore, many researchers have endeavored to find out sequences forming G-triplexes (G3s) that have three-stranded noncanonical secondary structure and similar biochemical functions like G4s but relatively less stability than G4s [12, 14–16]. For example, a truncated form of the G4 sequence thrombin binding aptamer (TBA), TBA11 (11-nt sequence, 5′-GGTTGGTGTGG-3′), was obtained and found to be able to fold into a G3 structure [14, 15, 17]. TBA11 has been proved to interact with hemin and can significantly

Shanshan Qin and Xuliang Chen contributed equally to this work.

✉ Ying Li
liying@wipm.ac.cn

✉ Yunhuang Yang
yang_yh@wipm.ac.cn

1 State Key Laboratory of Magnetic Resonance and Atomic Molecular Physics, National Centre for Magnetic Resonance in Wuhan, Wuhan Institute of Physics and Mathematics, Innovation Academy for Precision Measurement Science and Technology - Wuhan National Laboratory for Optoelectronics, Chinese Academy of Sciences, Wuhan 430071, China

2 University of Chinese Academy of Sciences, Beijing 10049, China

3 Department of Cardiovascular Surgery, Xiangya Hospital, Central South University, Changsha 410008, China

4 Wuhan National Laboratory for Optoelectronics, Huazhong University of Science and Technology, Wuhan 430074, Hubei, China

enhance the peroxidase-like activity of hemin [18]. Zhou et al. selected out an optimal G3-forming sequence from 14 G-rich sequences to design a G3-based MB for microRNA detection [11]. Other several G3 sequences have also been screened and identified with promising properties such as owning Amplex Red Oxidase activity [19, 20], lighting up ThT, and showing strong affinity with methylene blue [12].

As we know, human telomere G4 (ht-G4) formed by tandem repeats of the TTAGGG sequence has been intensively studied due to its direct relevance in inhibiting the telomerase activity and good performance in biosensing technology [21]. For example, AG22 (5′-AGGGTTAGG GTTAGGGTTAGGG-3′) has been recognized as one of the most efficient G4s to promote ThT to produce fluorescence and many biosensors have been developed by using it as the reporter. However, limited studies have been found working on the human telomeric sequence (5′-TTAGGGTTAGGG TTAGGGTTA-3′) though this oligonucleotide has already been approved to be able to form the G3 structure since 2012 [22]. Instead of screening potential G3 sequences, we studied the properties of this existed ht-G3 structure and found out that it could efficiently light up ThT in potassium solution. We also established an RNA detection strategy by designing an ht-G3-based MB and implemented it for the detection of SARS-CoV-2. The limit of detection (LOD) reached 0.01 nM when combined with a target recycling strategy. We anticipate this simple, sensitive, and label-free detection method to be widely used in RNA testing.

Experimental

Materials

All the DNA and RNA sequences (listed in Table S1) were obtained from Tsingke company (Beijing, China). The oligonucleotides were dissolved in water and heated at 95 ℃ for 5 min and cooled down to room temperature before use. If not specifically mentioned, the oligonucleotides were diluted to the desired concentrations by using the buffer (10 mM Tris–HCl, 50 mM K^+, pH 7.9). ThT was purchased from Aladdin Biochemical Technology Co., Ltd. (Shanghai, China). Duplex-specific nuclease (DSN) was purchased from NEWBORNCO., Ltd. (Shenzhen, China). RNase inhibitor was obtained from Vazyme (Jiangsu, China).

Methods

Circular dichroism experiments

Circular dichroism (CD) experiments were carried out on Chriascan (Applied Photophysics, UK). The data were collected in a cuvette (300 μL) with a path length of 0.1 cm. The average of three scans was recorded at room temperature at a scanning rate of 100 nm/min, from 220 to 320 nm (~ 25 ℃). The CD spectra of ht-G3 (final concentration, 5 μM) in a Tris buffer that contains 50 mM K^+ or 50 mM Na^+ were measured. All spectra were corrected with matching buffer blanks.

Measurement of fluorescence spectroscopy

Fluorescence resonance energy transfer (FRET) assay was performed to explore the G3 structure formed in 50 mM K^+ or Na^+. To carry out the assay, the 5′-FAM- and 3′-TAMRA-labeled G3 sequences were diluted to a final concentration of 25 nM. Fluorescence measurements were performed on a FluoroMax-4 spectrofluorometer (Horiba, Japan) at room temperature. The excitation and emission slits were set as 7 nm. Excitation was set at 488 nm, and emission was collected from 500 to 750 nm.

To study the properties of ht-G3 for lighting up ThT, a series of experiments was performed. First, the fluorescence intensity of ThT (6 μM) alone in 50-, 100-, and 200-mM Na^+ or K^+ buffer was measured, respectively, to explore the influence of the two monovalent ions. Then, ht-G3 (100 μL, 1 μM) was incubated with ThT (180 μL, 10 μM) for 2 h in a total of 300 μL Tris–HCl buffer containing 50-, 100-, and 200-mM Na^+ or K^+, respectively, to optimize the reaction condition for ht-G3 lighting up ThT. For the measurement of ThT fluorescence, the excitation and emission slits were set as 7 nm. Excitation was set at 420 nm, and emission was collected from 450 to 600 nm.

Design and selection of the ht-G3-based MB (ht-G3MB)

Target RNA was chosen from the specific sequences of the SARS-CoV-2 N-gene. To meet the basic requirement of the MB, we selected four sequences from the N-gene and designed the relevant ht-G3MB. The secondary structure of these MBs was predicted by DNAMAN 7.0 (Lynnon Biosof, USA). After the theoretical analysis, ht-G3MB1 and ht-G3MB2 with potentially better performance were synthesized and tested. ht-G3MB1 and ht-G3MB2 (30 μL, 1 μM) were mixed with their relevant targets RNA1 and RNA2, respectively, in the buffer with a total volume of 282 μL and incubated for 20 min at room temperature. Then, ThT (18 μL, 100 μM) was added into the mixture and incubated for 2 h. Then, the fluorescence of the solution was measured.

Specificity and LOD test of the ht-G3MB-based strategy

To test the specificity, RNA1 or RNA2 (30 μL, 10 nM) and ht-G3MB1 (30 μL, 1 μM) were mixed in the buffer

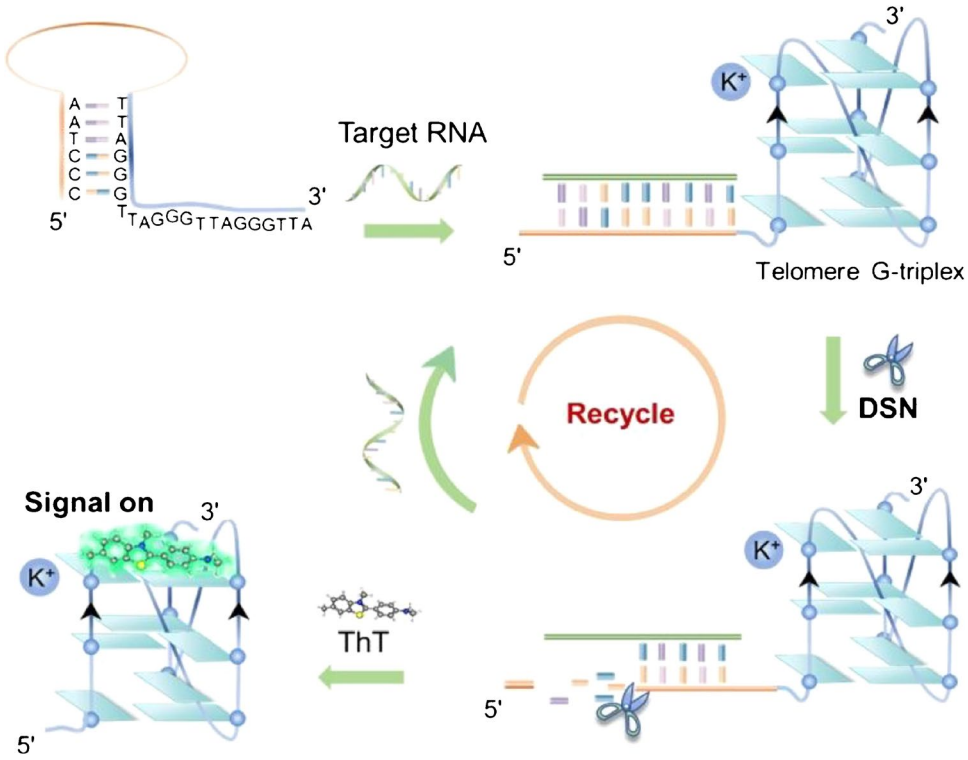

Scheme 1 Schematic illustration of the ht-G3-based MB for target RNA detection

with a total volume of 282 µL and incubated for 20 min at room temperature. Then, ThT (18 µL, 100 µM) was added into the mixture and incubated for 2 h. Then, the fluorescence of the solution was measured.

Next, a series of RNA1 samples was prepared with concentrations from 0 to 300 nM and tested to explore the LOD of this method. The reagents were mixed and incubated as mentioned above for 2 h. Then, the fluorescence of the solution was measured.

DSN–based target recycling strategy for RNA detection

To test the function of DSN for target recycling and signal amplification, we added DSN into the detection system. ht-G3MB1 (1.5 µL, 1 µM), different concentrations of RNA1, DSN (30 µL, 1 µM), and RNase inhibitor (2.5 µL, 40 U/µL) were mixed in 46 µL DSN storage buffer (10 mM Tris, 50 mM K^+, 1 mM DTT, 5 mM Mg^{2+}, pH 7.9) at 60 °C for 40 min. Then, ThT (1 µL, 100 µM) was added into this mixture and diluted to 150 µL. After incubation for 2 h, the fluorescence was measured via a microplate reader (SpectraMax i3x, Molecular Devices, CA, USA). The excitation wavelength was set as 420 nm, and the emission was collected from 450 to 600 nm.

Results and discussion

Scheme of the RNA detection strategy

As shown in Scheme 1, we propose a label-free RNA detection strategy based on the finding that ht-G3 lights up ThT. Initially, a DNA molecular beacon (MB) is designed containing three fragments: an ht-G3 sequence at the 3′ end, a loop that recognizes the RNA target, and a sequence at the 5′ end complementary to part of the G3 sequence. When there is RNA target presented, the loop region will bind with the target to form hybrid DNA-RNA double strands, which opens the stem region to release the G3 sequence. In K^+ buffer, the reduplicated TTAGGG sequence self-assembles into a G3 structure. To increase the detection sensitivity of this strategy, duplex-specific nuclease (DSN) is introduced into the system to recycle the RNA target. DSN is an enzyme that can efficiently cut DNA in double-stranded DNA (dsDNA) or hybrid double strands of DNA-RNA, but not cleave RNA or single-stranded DNA [12]. For signal detection, ThT is added into the reaction system and bright fluorescence will be obtained due to ht-G3 lighting up ThT. Therefore, this strategy offers a way to detect RNA target in a label-free mode.

Investigation of ht-G3 lighting up ThT

We first checked the G3 structure formation in K^+ and Na^+ buffer. We labeled the ht-G3 sequence with FAM and TAMRA at the two ends (Table S1) and measured the fluorescence spectrum. Fluorescence resonance energy transfer (FRET) efficiency between the donor (FAM) and acceptor (TAMRA) in some extent reveals the conformational changes of the oligonucleotide, which can be expressed using the proximity ratio $I = Ia/(Ia + Id)$ [23], where *Ia* and *Id* are the fluorescence intensities of the acceptor and the donor, respectively. In the buffer solution without monovalent metal ions (Fig. 1a), the FRET signal was very low (~0.25). However, the FRET efficiency significantly increased to 0.59 and 0.64 in the solution with Na^+ and K^+, respectively [16, 24, 25]. This result revealed that the ht-G3 sequence formed a higher-order structure that resulted in the approaching of the two fluorescent probes. Then, we used circular dichroism (CD) to further examine the formation of the triplex structure. As shown in Fig. 1b, the ht-G3 sequence formed a parallel/antiparallel hybrid G3 structure in solution with K^+, similar to that of K^+-induced ht-G4 [26]. The CD spectrum of ht-G3 in solution with Na^+ shows a clear peak at 257 nm and a valley at 238 nm (highly consistent with the G3 reported in the literature) [22], which is significantly different from Na^+-induced ht-G4 that has a strong negative peak at 265 nm and a strong positive peak at 295 nm. These CD results further proved that this telomere G-rich sequence formed the G3 structure in K^+ and Na^+ buffer.

Then, we moved to study the performance of K^+- and Na^+-induced ht-G3 for lighting up ThT. Before the testing, the influence of K^+/Na^+ concentrations on ThT fluorescence was checked. As shown in Fig. 1c, no significant effect was found when comparing the control (ThT without K^+/Na^+) and the solutions with different K^+/Na^+ concentrations, though the fluorescence intensity of ThT increased in some degree in the 200-mM Na^+ solution. Then, we analyzed the fluorescence of ThT when there was ht-G3 in the solution with different K^+/Na^+ concentrations. Figure 1d illustrates that ht-G3 significantly lighted up ThT since the fluorescence intensity was apparently higher when ht-G3 presented in the solution. Moreover, K^+-induced ht-G3 was more efficient to promote the fluorescence production of ThT. Meanwhile, we did not find significant influence of the monovalent ion concentrations on the fluorescence of ThT. Thus, we used 50 mM K^+ in the reaction buffer in all the subsequent experiments. Thereafter, we compared the performance of ht-G3 and TBA11 (a typical G3-forming sequence in potassium solution) for lighting up ThT. As shown in Figure S1a, ht-G3 demonstrated much better performance than TBA11. Additionally, we also found that ThT fluorescence increased significantly when ht-G3 concentration increased (Figure S1b), which means that it should be reasonable by using ht-G3 as a probe for target detection.

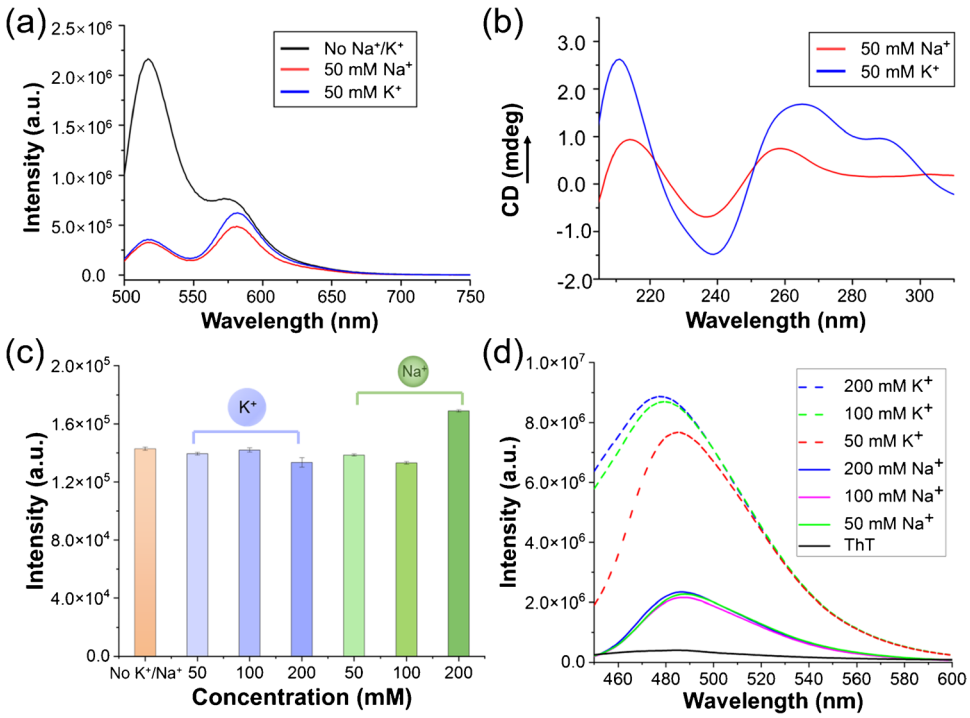

Fig. 1 Investigation of ht-G3 lighting up ThT. **a** Fluorescence spectra of ht-G3. **b** CD spectra of ht-G3. **c** Influence of $K^+/Na.^+$ concentrations on the fluorescence intensity of ThT (without ht-G3). **d** The fluorescence spectrum of ThT (with ht-G3) in different buffer solutions. "ThT" represents no ht-G3 was added

Designing of the ht-G3MB

After testing the efficiency of ht-G3 for lightening ThT, we moved to design the ht-G3-based MB (ht-G3MB) for RNA detection. Herein, we chose SARS-CoV-2 N-gene as the target. The ht-G3MB contains three parts: the G3 sequence, a loop (to be paired with the target), and a short sequence paring with part of the G3 sequence to form a stem and inhibit the G3 formation. DSN is known to be able to cleave DNA duplexes down to ~ 10 bp size [27], and additional studies demonstrated that double strands with size of less than 7 bp could efficiently avoid the cleavage by DSN. In consideration of these features of DSN [28, 29], the stem length of the ht-G3MB is designed as 6 base pairs to avoid DSN cleavage and also enable well locking of the G3 structure. Additionally, the loop region is designed according to the target RNA. We did a full-length screening on the specific sequence of the SARS-CoV-2 N-gene and searched out four sequences that could meet the basic requirements. We then used DNAMAN 7.0 [30] (a computer software) to investigate the high-order structure of the ht-G3MB to check whether the screened sequences could form the anticipated hairpin structure. The predicted result by DNAMAN showed that one of the four sequences (ht-G3MB1) formed the designated hairpin structure, while the other three formed an additional hairpin structure (Fig. 2). Anyway, we synthesized ht-G3MB1, ht-G3MB2 (as a backup), and their relevant RNA targets to verify their experimental performance.

Detection sensitivity of the ht-G3MB-based strategy for RNA detection

We first checked whether the synthesized ht-G3MB could be locked before adding the RNA target. As shown in Figure S2, the testing results demonstrated that ht-G3MB1 was locked well since the fluorescence intensity of ThT only increased slightly, while ht-G3MB2 already activated ThT and resulted in bright fluorescence in the absence of target. These results revealed that ht-G3MB1 should be an optimum MB and much better than ht-G3MB2 for RNA detection, which is consistent with the software prediction (Fig. 2) and the results in the polyacrylamide gel electrophoresis characterization (Figure S3). We then applied ht-G3MB1 to detect the target RNA1. The result in Fig. 3b demonstrates that the fluorescence significantly increased after adding RNA1, verifying the performance of this ht-G3-based MB. Additionally, RNA1 and RNA2 (the RNA target designated for ht-G3MB2) were used to test the specificity of ht-G3MB1, and the results are shown in Fig. 3c. It displayed that the optimum MB owned a good specificity for discriminating RNA1 and RNA2. Furthermore, we used this strategy to detect RNA1 with a series of concentrations. The results in Fig. 3d show that the detection limit for this MB-based strategy (without DSN cleavage for target recycling) is about 1 nM, comparable to that reported in the literature that selected a stable G3 sequence to build the MB [11].

Characterization of the DSN-based target recycling detection strategy

To further increase the sensitivity, we introduced DSN into the detection system. As shown in Fig. 4a, DSN can destroy the DNA segment paring with the RNA target and release the target for recycling and signal amplification; thus, it should be helpful to improve the detection limit. We first evaluated the performance of the DSN by testing 1 nM RNA target. Figure S4 and Fig. 4b display that the fluorescence increased significantly when there was DSN in the reaction system, proving the function of DSN. Additionally, we further parallelly tested 0.1- and 1-nM RNA target with or without DSN. The results demonstrated that DSN could apparently promote

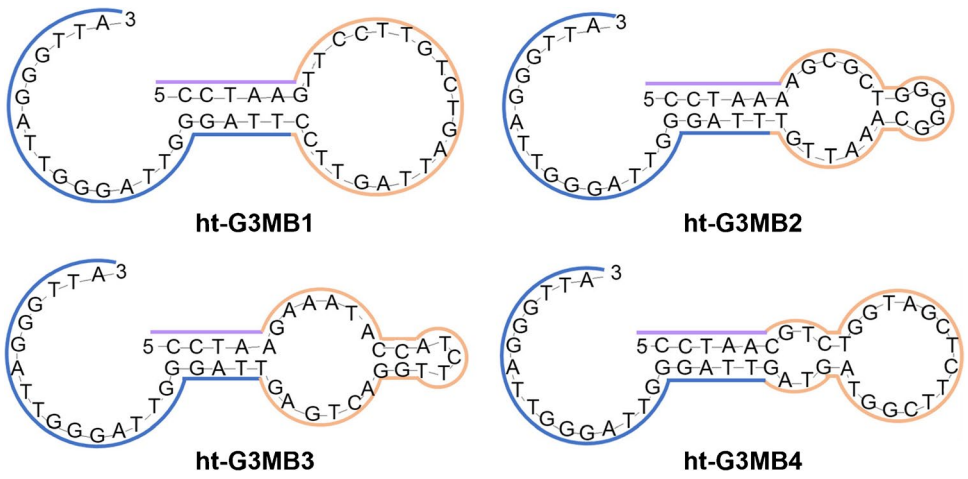

Fig. 2 Designed ht-G3MBs after a full-length screening on the specific sequence of SARS-CoV-2 N-gene. The molecular beacon contains the ht-G3 sequence at the 3′ end (blue line), the loop region that recognizes the RNA target (yellow line), and a sequence complementary to part of the G3 sequence (purple line)

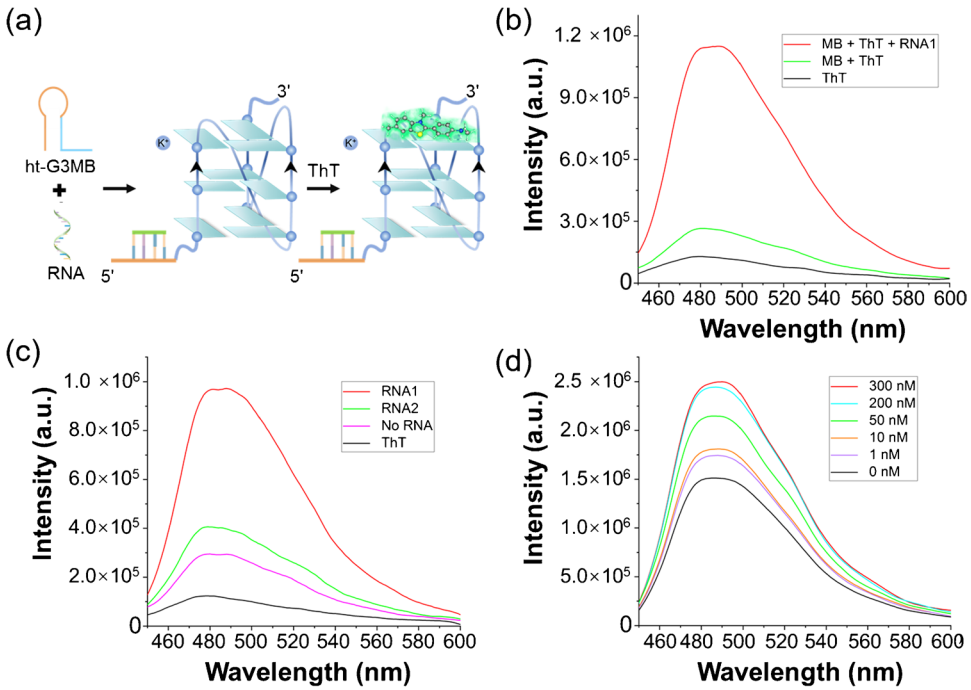

Fig. 3 Investigation of the ht-G3MB for target RNA detection. **a** Schematic illustration of the RNA detection. **b** Evaluation of the ht-G3MB/ThT for RNA detection. **c** Specificity test of the MBs. **d** Sensitivity test of the ht-G3MB1

the fluorescence production (Fig. 4c). Furthermore, we investigated the LOD of the ht-G3MB1-based strategy with DSN. The results shown in Fig. 4d revealed that 0.01 nM RNA can be distinguished from the buffer without target, suggesting that DSN improved the detection limit about 100 times for RNA detection. We believe this strategy could be applied to the detection of SARS-CoV-2 in clinical samples if combined with certain amplification strategies such as recombinase polymerase amplification [31].

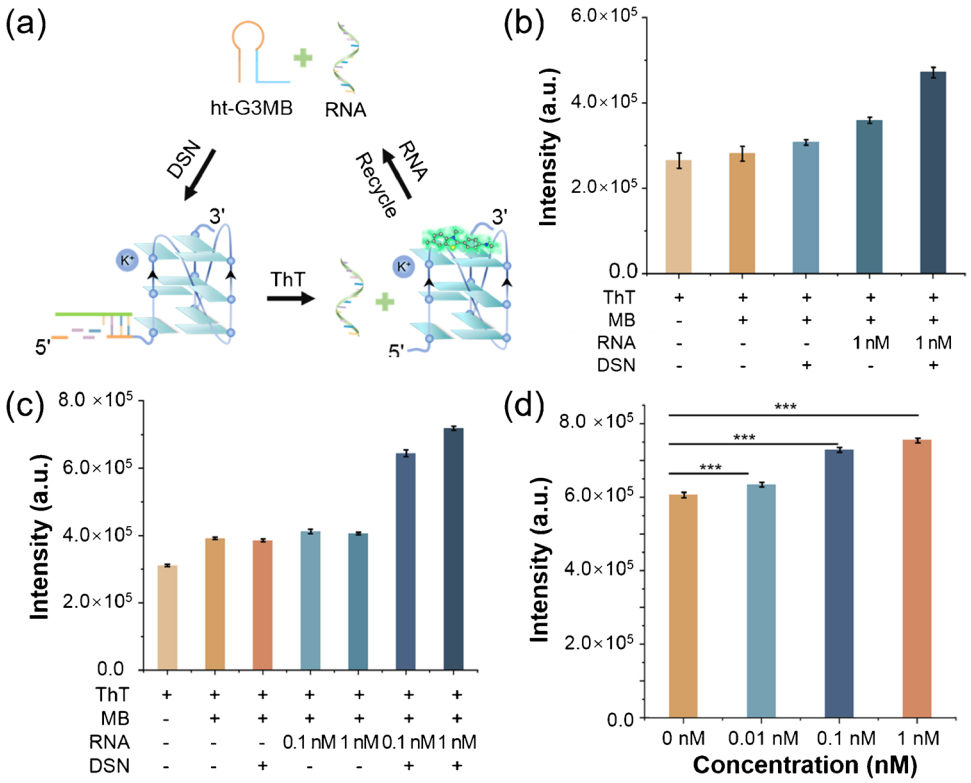

Fig. 4 DSN–based target recycling strategy for the detection of RNA1. **a** Scheme of the detection strategy. **b** Verification of the DSN–based strategy for signal amplification. **c** Performance comparison of the ht-G3MB1-based system in the presence or absence of DSN. **d** Detection limit of the DSN–based strategy. ***$P < 0.005$

Conclusion

In conclusion, we investigated the function of ht-G3 for lighting up ThT and developed an ht-G3-based MB for RNA detection. Our results demonstrated that K^+-induced ht-G3 formed a hybrid structure similar to ht-G4 and it can efficiently light up ThT. Based on this, we selected out an optimal ht-G3MB for label-free detection of the SRAS-Cov-2 N-gene. The detection limit was about 1 nM. By further introducing DSN for target recycling and signal amplification, the detection limit was improved 100 times down to 0.01 nM RNA. In this work, we did not try to screen new G3 sequences but investigated the performance of the existed ht-G3 and explored its function as a MB for label-free and sensitive nucleic acid detection. We expected ht-G3 and the relevant MB could be widely implemented in biosensing.

Supplementary Information The online version contains supplementary material available at https://doi.org/10.1007/s00216-022-04180-7.

Acknowledgements We gratefully acknowledge the financial support from the National Natural Science Foundation of China (22174150, 21904139, 21735007), Chinese Academy of Sciences (Y9Y1041001, YJKYYQ20170026).

The authors declare no conflicts of interest.

References

1. Spiegel J, Adhikari S, Balasubramanian S. The structure and function of DNA G-quadruplexes. Trends Chem. 2020;2(2):123–36.
2. Chen J, Cheng M, Salgado GF, Stadlbauer P, Zhang X, Amrane S, Guédin A, He F, Šponer J, Ju H, Mergny JL, Zhou J. The beginning and the end: flanking nucleotides induce a parallel G-quadruplex topology. Nucleic Acids Res. 2021;49(16):9548–59.
3. Macaya RF, Schultze P, Smith FW, Roe JA, Feigon J. Thrombin-binding DNA aptamer forms a unimolecular quadruplex structure in solution. Proc Natl Acad Sci USA. 1993;90(8):3745–9.
4. Rhodes D, Lipps HJ. G-quadruplexes and their regulatory roles in biology. Nucleic Acids Res. 2015;43(18):8627–37.
5. Zhao C, Qin G, Niu J, Wang Z, Wang C, Ren J, Qu X. Targeting RNA G-quadruplex in SARS-CoV-2: a promising therapeutic target for COVID-19? Angew Chem Int Ed Engl. 2021;60(1):432–8.
6. Masai H, Tanaka T. G-quadruplex DNA and RNA: their roles in regulation of DNA replication and other biological functions. Biochem Biophys Res Commun. 2020;531(1):25–38.
7. Métifiot M, Amrane S, Litvak S, Andreola ML. G-quadruplexes in viruses: function and potential therapeutic applications. Nucleic Acids Res. 2014;42(20):12352–66.
8. Zhang L, Chen J, He M, Su X. Molecular dynamics simulation-guided toehold mediated strand displacement probe for single-nucleotide variants detection. Exploration. 2022;2(1):20210265.
9. Wang J, Cheng M, Chen J, Ju H, Monchaud D, Mergny JL, Zhou J. An oxidatively damaged G-quadruplex/hemin DNAzyme. Chem Commun (Camb). 2020;56(12):1839–42.
10. Guan AJ, Zhang XF, Sun X, Li Q, Xiang JF, Wang LX, Lan L, Yang FM, Xu SJ, Guo XM, Tang YL. Ethyl-substitutive Thioflavin T as a highly-specific fluorescence probe for detecting G-quadruplex structure. Sci Rep. 2018;8(1):2666.
11. Zhou H, Wu ZF, Han QJ, Zhong HM, Peng JB, Li X, Fan XL. Stable and Label-Free Fluorescent Probe Based on G-triplex DNA and Thioflavin T. Anal Chem. 2018;90(5):3220–6.
12. Zhao LL, Cao T, Zhou QY, Zhang XH, Zhou YL, Yang L, Zhang XX. The Exploration of a New Stable G-Triplex DNA and Its Novel Function in Electrochemical Biosensing. Anal Chem. 2019;91(16):10731–7.
13. Gao J, Liu Q, Liu W, Jin Y, Li B. Comparative evaluation and design of a G-triplex/thioflavin T-based molecular beacon. Analyst. 2021;146(8):2567–73.
14. Limongelli V, De Tito S, Cerofolini L, Fragai M, Pagano B, Trotta R, Cosconati S, Marinelli L, Novellino E, Bertini I, Randazzo A, Luchinat C, Parrinello M. The G-triplex DNA. Angew Chem Int Ed Engl. 2013;52(8):2269–73.
15. Jiang HX, Cui Y, Zhao T, Fu HW, Koirala D, Punnoose JA, Kong DM, Mao H. Divalent cations and molecular crowding buffers stabilize G-triplex at physiologically relevant temperatures. Sci Rep. 2015;5:9255.
16. Li T, Hu R, Xia J, Xu Z, Chen D, Xi J, Liu BF, Zhu J, Li Y, Yang Y, Liu M. G-triplex: A new type of CRISPR-Cas12a reporter enabling highly sensitive nucleic acid detection. Biosens Bioelectron. 2021;187:113292.
17. Demkovičová E, Bauer Ľ, Krafčíková P, Tlučková K, Tóthova P, Halaganová A, Valušová E, Víglaský V. Telomeric G-quadruplexes: from human to tetrahymena repeats. J Nucleic Acids. 2017;2017:9170371.
18. Wang S, Fu B, Peng S, Zhang X, Tian T, Zhou X. The G-triplex DNA could function as a new variety of DNA peroxidase. Chem Commun (Camb). 2013;49(72):7920–2.
19. Lin X, Chen Q, Liu W, Li H, Lin JM. A portable microchip for ultrasensitive and high-throughput assay of thrombin by rolling circle amplification and hemin/G-quadruplex system. Biosens Bioelectron. 2014;56:71–6.
20. Wang S, Fu B, Wang J, Long Y, Zhang X, Peng S, Guo P, Tian T, Zhou X. Novel amplex red oxidases based on noncanonical DNA structures: property studies and applications in microRNA detection. Anal Chem. 2014;86(6):2925–30.
21. Sun L, Zhao Q, Liu X, Pan Y, Gao Y, Yang J, Wang Y, Song Y. Enzyme-mimicking accelerated signal enhancement for visually multiplexed quantitation of telomerase activity. Chem Commun (Camb). 2020;56(51):6969–72.
22. Koirala D, Mashimo T, Sannohe Y, Yu Z, Mao H, Sugiyama H. Intramolecular folding in three tandem guanine repeats of human telomeric DNA. Chem Commun (Camb). 2012;48(14):2006–8.
23. Green JJ, Ying L, Klenerman D, Balasubramanian S. Kinetics of unfolding the human telomeric DNA quadruplex using a PNA trap. J Am Chem Soc. 2003;125(13):3763–7.
24. Li Y, Li T, Liu BF, Hu R, Zhu J, He T, Zhou X, Li C, Yang Y, Liu M. CRISPR-Cas12a trans-cleaves DNA G-quadruplexes. Chem Commun (Camb). 2020;56(83):12526–9.
25. Li Y, Liu C, Feng X, Xu Y, Liu BF. Ultrafast microfluidic mixer for tracking the early folding kinetics of human telomere G-quadruplex. Anal Chem. 2014;86(9):4333–9.
26. Ambrus A, Chen D, Dai J, Bialis T, Jones RA, Yang D. Human telomeric sequence forms a hybrid-type intramolecular G-quadruplex structure with mixed parallel/antiparallel strands in potassium solution. Nucleic Acids Res. 2006;34(9):2723–35.
27. Zhao Y, Hoshiyama H, Shay JW, Wright WE. Quantitative telomeric overhang determination using a double-strand specific nuclease. Nucleic Acids Res. 2008;36(3):e14.
28. Wu Z, Zhou H, He J, Li M, Ma X, Xue J, Li X, Fan X. G-triplex based molecular beacon with duplex-specific nuclease

amplification for the specific detection of microRNA. Analyst. 2019;144(17):5201–6.
29. Moazampour M, Zare HR, Shekari Z. Femtomolar determination of an ovarian cancer biomarker (miR-200a) in blood plasma using a label free electrochemical biosensor based on L-cysteine functionalized ZnS quantum dots. Anal Methods. 2021;13(17):2021–9.
30. Wang ZH, Fang SG, Xu JL, Sun LY, Li DW, Yu JL. Sequence analysis of the complete genome of rice black-streaked dwarf virus isolated from maize with rough dwarf disease. Virus Genes. 2003;27(2):163–8.
31. Broughton JP, Deng X, Yu G, Fasching CL, Servellita V, Singh J, Miao X, Streithorst JA, Granados A, Sotomayor-Gonzalez A, Zorn K, Gopez A, Hsu E, Gu W, Miller S, Pan CY, Guevara H, Wadford DA, Chen JS, Chiu CY. CRISPR-Cas12-based detection of SARS-CoV-2. Nat Biotechnol. 2020;38(7):870–4.